Electron Interferometry at a Metal-Semiconductor Interface

J. A. Kubby and W. J. Greene
Xerox Webster Research Center, 800 Phillips Road, Webster, New York 14580
(Received 17 September 1991)

The tunneling microscope is used to excite electron standing waves at the $NiSi_2/Si(111)$ metal-semiconductor interface. Conductivity mappings show contrast between type-A and type-B domains of nickel disilicide, as well as contrast between domains of type-B disilicide of varying thicknesses. We demonstrate the presence of buried steps, and that these steps can act as diffusion barriers in the reaction that leads to the formation of the nickel disilicide overlayer.

PACS numbers: 61.16.Di, 68.35.−p, 73.20.−r, 73.30.+y

As our understanding of the vacuum-solid interface becomes more complete, interest has increased in characterizing the solid-solid interface. While such interfaces play an important role in determining the properties of semiconductor devices such as the Schottky barrier height of a metal-semiconductor contact [1] or level broadening due to interface roughness in quantum well devices, determining the real-space properties of an interface on an atomic scale is difficult as the buried interface is not directly accessible to the principal surface science structural probes. In this Letter we demonstrate that the scanning tunneling microscope (STM) can be used for atomic scale characterization of the buried $NiSi_2/Si(111)$ metal-semiconductor interface, utilizing the technique of electron standing-wave interferometry [2–5].

The nickel disilicide system is ideal for such studies as epitaxial films of $NiSi_2$ form atomically abrupt and structurally perfect metal-semiconductor interfaces [6]. Furthermore, by controlling growth kinetics [6], it is possible to form disilicide films with two different orientations relative to the substrate lattice, allowing a comparison of interface structural effects on standing-wave formation.

We demonstrate that it is possible to observe buried step structure associated with thickness fluctuations of the thin $NiSi_2$ film. We show that such buried steps often separate domains of different silicon adatom densities, which has implications for the role of diffusion barriers in the nucleation and growth kinetics of these films. Finally, we demonstrate that it is possible to observe conductivity contrast between the two orientations of $NiSi_2$ on $Si(111)$: type A, in which the silicide has the same orientation as the substrate, and type B, in which the silicide shares the surface normal $\langle 111\rangle$ axis with the silicon lattice but is rotated 180° about this axis with respect to the substrate. The three-terminal technique of ballistic electron emission microscopy (BEEM) [7] has recently been used to characterize mixed phases of type-A and -B nickel disilicides with clean and atomically flat surfaces under ultrahigh vacuum conditions. However, the difference of BEEM currents between types A and B, that should reflect differences in the Schottky barrier height between these two orientations [1], was found to be quite small and within the expected statistical fluctuation, and thus unable to differentiate between type-A and -B buried interfaces [8]. On the other hand, the electron interferometry technique described here, where the contrast mechanism is sensitive to the reflectivity of the interface [4,5], clearly resolves differences between these two domains.

The samples were cut from an arsenic-doped 0.005-Ω cm $Si(111)$ wafer, and prepared *ex situ* with a thin passivating oxide. The oxide was sublimated *in situ* at 875 °C by passing a direct current through the well outgassed specimen. Nickel was deposited at a rate of 0.8 Å/min from an e-beam source, onto a room-temperature $Si(111)$-7×7 surface. The samples were then heated to 500 °C for 3 to 5 min, after which they displayed sharp (1×1) LEED patterns with threefold symmetry, having different intensities for the (1,0) and $(\bar{1},0)$ beams. The relative intensities of the two types of spots depended on the amount of deposited Ni, which was monitored with a crystal oscillator. The variation of $NiSi_2$ orientation as a function of deposited nickel thickness was found to be in agreement with the template method of Tung, Gibson, and Poate [6] for depositions in the range from 4 to 20 Å. The operation of the microscope to obtain conductivity spectra and conductance mappings has been described previously [2,3].

Figure 1 shows a topographic image of the nickel disilicide surface that results from an initial nickel deposition of 20 Å. The surface consists of a sixfold (1×1) mesh with a nearest-neighbor distance of 3.8 Å, and triangular silicon adatom islands with vertices that are all oriented along the $\langle\bar{1}\bar{1}2\rangle$ crystallographic directions of the silicon substrate. Two terraces are shown, separated by a 6.2-Å double height step, that has an outward normal along the $\langle 11\bar{2}\rangle$ direction. The type of interface that has been formed can be determined by noting the orientation of the triangular adatom islands relative to the $\langle\bar{1}\bar{1}2\rangle$ direction of the silicon lattice, determined prior to nickel deposition [3]. The triangular adatom islands are always oriented along the $\langle\bar{1}\bar{1}2\rangle$ directions of the silicide [8,9]. Since the $\langle\bar{1}\bar{1}2\rangle$ direction of the silicide shown in Fig. 1 points along the $\langle\bar{1}\bar{1}2\rangle$ direction of the silicon substrate, this is a pure type-A domain of nickel disilicide. A type-B domain would be rotated by 180° and would have triangular adatom islands oriented along the $\langle 11\bar{2}\rangle$ directions of the silicon substrate. Surfaces with mixed $A+B$ regions would have triangular adatom islands pointing in

© 1992 The American Physical Society

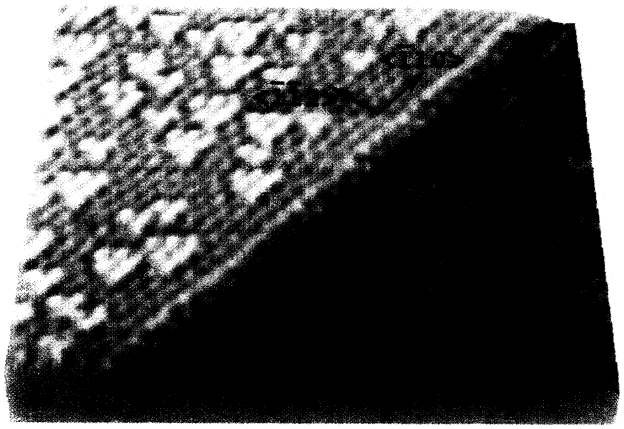

FIG. 1. STM topograph (125×125 Å) of a type-A $NiSi_2(111)$ surface at a tip bias of −0.6 eV, 1.0 nA. Adatoms form triangular islands that are oriented along the $\langle \bar{1}\bar{1}2 \rangle$ directions of the underlying silicon lattice.

opposite directions, as shown in Fig. 2.

Figure 2(a) shows a region containing a mixture of type-A and -B domains that results from an initial 7.5-Å Ni deposition. The various domains have been labeled in Fig. 2(b); domain I is type A, and domains II and III are type B. The image consists of two terraces, separated by an 18.6-Å step. In these larger images the (1×1) $NiSi_2$ mesh is no longer discernible; however, the adatom trimers can still be resolved. The domain boundary between the type-A and -B regions on the lower terrace of Fig. 2(a) runs along the $\langle 0\bar{1}1 \rangle$ [marked g in Fig. 2(c)] and $\langle \bar{1}10 \rangle$ [marked h in Fig. 2(c)] directions and is decorated with adatoms. There is a slight height difference between these two domains, with region II higher than region I by 0.15 Å at a tip bias of −1.0 eV, which will be discussed below. This height difference, as well as the relative orientation of the silicon trimers on either side of the domain boundary is emphasized in the inset shown in Fig. 2(a). In Fig. 2(c), a conductivity map at −1.0 eV is shown, that was collected simultaneously with the topographic map in Fig. 2(a). The light area indicates a region of high conductivity, which is mostly confined to the type-B domain in region II. The high-conductivity region extends slightly into the type-A region (I) along the $\langle 0\bar{1}1 \rangle$ part of the domain boundary [g in 2(c)] but not along the $\langle \bar{1}10 \rangle$ part [h in 2(c)], indicating that these are not equivalent transitions. To see the spatial relationship between the topographic and conductance mappings, they have been rendered in color (topography, blue; conductance, orange) with the overlay of these two images shown in Fig. 2(b). The conductivity of the type-B domain (III) above the step is not equivalent to the conductivity of the type-B domain (II) below the step. We attribute this contrast to a difference in the nickel disilicide film thickness as discussed below. In addition, the conductivity of the type-B domain in region II is not equivalent to the conductivity of the type-A domain in region I, even though both domains are in the same terrace.

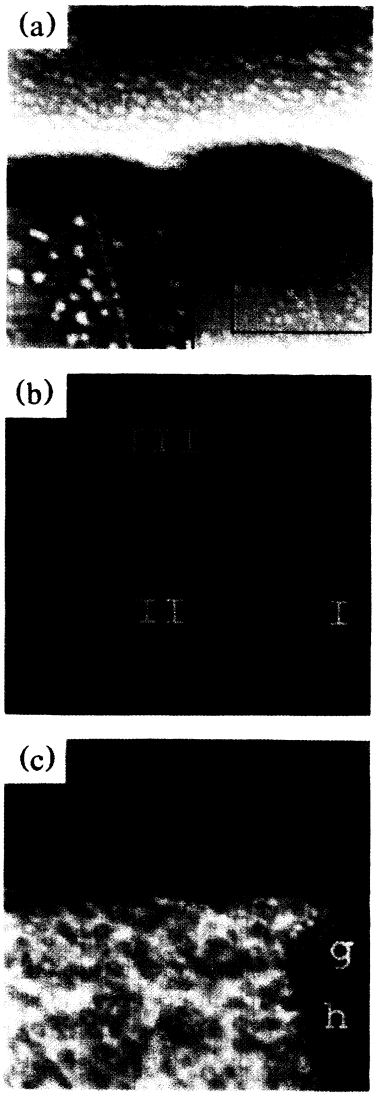

FIG. 2. STM topographic and conductance images (360×360 Å) of type-A and -B domains at a tip bias of −1.0 eV, 1 nA. (a) Topographic image, (b) overlay image (topography, blue; conductance, orange), and (c) conductance image. The type-A domain is labeled I and the type-B domains are labeled II and III in (b). The $\langle 0\bar{1}1 \rangle$ and $\langle \bar{1}10 \rangle$ parts of the A/B domain boundary have been labeled g and h, respectively, in (c). The inset shown in (a) is a magnified view of the area outlined by the box.

Two different sources of conductivity contrast between the A and B domains are possible. First, structural differences between the buried A and B interfaces could lead to differences in electron transmission through the different interface orientations [10]. These differences would lead to differences in the formation of electron standing waves that arise from the reflection of electrons at these interfaces. As the type-B interface is predicted to be more strongly reflecting than the type-A interface [10], the formation of electron standing waves from elec-

tron reflections off of a type-*B* interface should be stronger than from a type-*A* interface. The effect of standing-wave formation on topographic and conductance mappings is discussed below.

A structural analogy can be drawn between the *A* and *B* disilicide interfaces and the interfaces formed by the two types of triangles inside a silicon Si(111)-7×7 unit cell [11]. Both the type-*B* disilicide and the faulted Si(111)-7×7 triangle are formed by a twist of the lattice about the ⟨111⟩ axis normal to the interface, whereas the type-*A* disilicide and the unfaulted Si(111)-7×7 triangle are not twisted. It has previously been shown that the stacking fault on a Si(111)-7×7 surface gives rise to topographic and conductance contrast at particular resonant biases [3,5]. These biases correspond to the energies at which electron standing waves form between the surface and buried twist interface. Near a resonance, the conductance map renders contrast indicating an increase in the density of final states associated with the formation of an electron standing wave. The transmission coefficient through the interface also increases due to a Fabry-Pérot transmission resonance when the electronic phase changes by 2π on a full circuit of the region between the surface and twist interface [12,13]. On resonance the faulted region of the unit cell appears to be 0.1 Å higher than the unfaulted region in topographic maps, as the formation of an electron standing wave within the faulted region leads to an increase in the density of states; there is one extra allowed final state within the faulted region at resonance [5]. Thus, in analogy to the faulted triangle of the Si(111)-7×7 unit cell, the type-*B* domain of nickel disilicide would be expected to render contrast in conductance mappings as a standing-wave resonance is approached, and to appear slightly higher than type-*A* domains in topographic images collected at resonant biases. Indeed, the apparent height of the type-*B* domain is 0.15 Å higher than the type-*A* domain in the inset to Fig. 2(a). Confirmation of this structural contrast mechanism will require comparison of experimental results with a calculation of electron transmission through thin films of type-*A* and type-*B* disilicide over a 10-eV energy interval, which would take into account the possibility of standing-wave formation between the surface and buried interfaces. A second possibility is that there is a buried step at the $NiSi_2$/Si(111) interface leading to a difference in thickness, and thus standing-wave boundary conditions [4,5] between regions I and II. This contrast mechanism is considered further in analyzing the conductivity contrast found in Fig. 3.

Figure 3(a) is a topographic image of a region containing two terraces of type-*B* nickel disilicide, separated by a 6.2-Å double height step. Figure 3(c) is a conductivity map at −0.6-eV bias that was collected simultaneously. There are four different conductivity levels within this image, that have been labeled I–IV. An overlay of these two images (topography, blue; conductance, orange) is shown in Fig. 3(b). *Since all of these domains are type B, the differences in conductivity contrast must arise from thickness fluctuations between the different domains.* The resonance energies of thin-film standing-wave states have been found [5] to vary almost as $(n/w)^2$ for the nth-order standing-wave state in a film of thickness w, and thus the conductivity fluctuations associated with excitation of thin-film standing-wave states are a sensitive measure of thickness fluctuations [4,5]. The relevant film thicknesses are expected to be integral multiples of 3.1-Å trilayer widths, as required by the $NiSi_2$ stoichiometry. Some calculated level spacings between the first two standing-wave states (using $m^*/m=1$) would be 11.7, 2.9, 1.3, and 0.7 eV for film thicknesses of 3.1, 6.2, 9.3, and 12.4 Å. Density-of-state features with

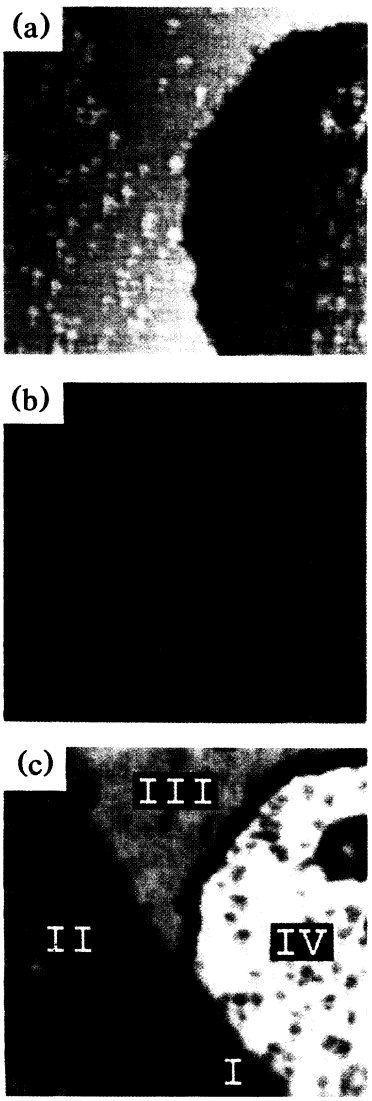

FIG. 3. STM and conductance images (360×360 Å) of type-*B* domains. (a) Topographic image, (b) overlay image (topography, blue; conductance, orange), and (c) conductance image at −0.6 eV, 1 nA. Type-*B* domains of varying thickness have been labeled I–IV.

these approximate level spacings have been observed in standing-wave dI/dV spectra [14].

The domain boundary between regions I and II as well as between regions III and IV is the double height step between the two surface terraces shown in Fig. 3(a). The domain boundary between regions II and III as well as between regions I and IV does not correspond to a step in the surface topography, and must then correspond to a step buried below the surface. *To the best of our knowledge this is the first detection of buried step structure with the tunneling microscope.*

A further observation is that the adatom trimer surface concentration is much higher in region II relative to region III. Similar differences in adatom concentration between type-*B* domains separated by buried steps have been observed in many other images, suggesting that it is a general trend. The adatom concentration difference suggests that the buried steps act as diffusion barriers for excess silicon between regions of different reaction depth; regions with higher adatom concentration result from nucleation conditions further off stoichiometry from $NiSi_2$.

In summary, we have used the tunneling microscope to perform electron interferometry at a $NiSi_2/Si(111)$ metal-semiconductor interface. We have detected conductivity contrast between type-*A* and type-*B* domains that coexist on a single terrace, and between regions of varying film thicknesses on pure type-*B* domains. We have demonstrated that the tunneling microscope can be used to image buried step structure, and that such structures can act as diffusion barriers for excess silicon adatoms left over from the reaction $Ni+2Si \rightarrow NiSi_2$.

We thank R. S. Becker at AT&T Bell Laboratories for useful discussions and for sharing the code used to render STM images, and G. M. Couto for graphics programming. We also thank T. E. Orlowski, R. E. Viturro, R. G. Dandrea, and L. C. Pizzo for comments and help in preparing the manuscript.

[1] R. T. Tung, Phys. Rev. Lett. **52**, 461 (1984).
[2] R. S. Becker, J. A. Golovchenko, and B. S. Swartzentruber, Phys. Rev. Lett. **55**, 987 (1985).
[3] R. S. Becker, J. A. Golovchenko, D. R. Hamann, and B. S. Swartzentruber, Phys. Rev. Lett. **55**, 2032 (1985).
[4] J. A. Kubby, Y. R. Wang, and W. J. Greene, Phys. Rev. Lett. **65**, 2165 (1990).
[5] J. A. Kubby, Y. R. Wang, and W. J. Greene, Phys. Rev. B **43**, 9346 (1991).
[6] R. T. Tung, J. M. Gibson, and J. M. Poate, Phys. Rev. Lett. **50**, 429 (1983).
[7] W. J. Kaiser and L. D. Bell, Phys. Rev. Lett. **60**, 1406 (1988).
[8] Y. Hasegawa, Y. Kuk, R. T. Tung, P. J. Silverman, and T. Sakurai, J. Vac. Sci. Technol. B **9**, 578 (1991).
[9] J. Rowe, R. S. Becker, G. K. Wertheim, and R. T. Tung (to be published).
[10] M. D. Stiles and D. R. Hamann, Phys. Rev. B **40**, 1349 (1989).
[11] J.-J. Yeh, Appl. Phys. Lett. **55**, 1241 (1989).
[12] The existence of Fabry-Pérot transmission resonances for multiple reflections between silicon twist boundaries was shown in M. D. Stiles and D. R. Hamann, Phys. Rev. B **41**, 5280 (1990).
[13] Y. R. Wang, J. A. Kubby, and W. J. Greene, Mod. Phys. Lett. **5**, 1387 (1991).
[14] J. A. Kubby, Y. R. Wang, and W. J. Greene (to be published).

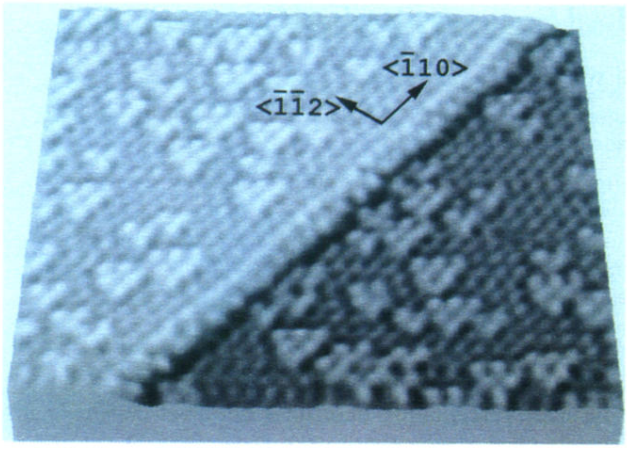

FIG. 1. STM topograph (125×125 Å) of a type-*A* $NiSi_2(111)$ surface at a tip bias of −0.6 eV, 1.0 nA. Adatoms form triangular islands that are oriented along the $\langle\bar{1}\bar{1}2\rangle$ directions of the underlying silicon lattice.

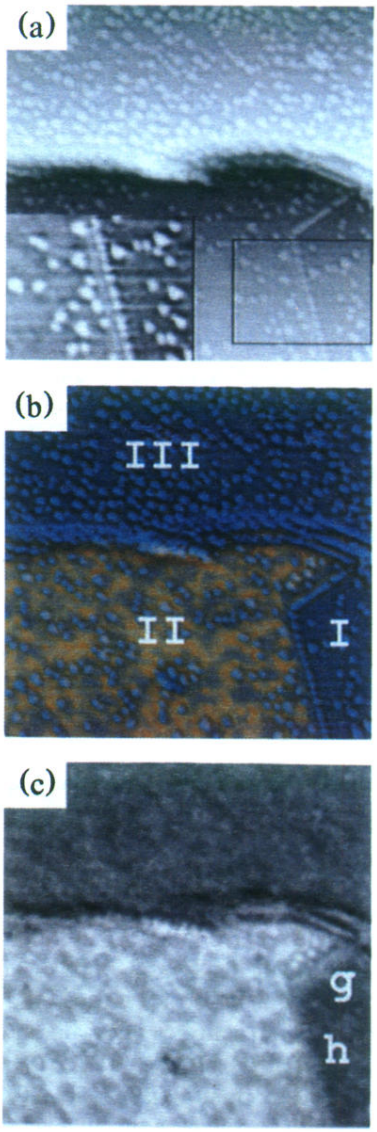

FIG. 2. STM topographic and conductance images (360×360 Å) of type-A and -B domains at a tip bias of −1.0 eV, 1 nA. (a) Topographic image, (b) overlay image (topography, blue; conductance, orange), and (c) conductance image. The type-A domain is labeled I and the type-B domains are labeled II and III in (b). The $\langle 0\bar{1}1\rangle$ and $\langle \bar{1}10\rangle$ parts of the A/B domain boundary have been labeled g and h, respectively, in (c). The inset shown in (a) is a magnified view of the area outlined by the box.

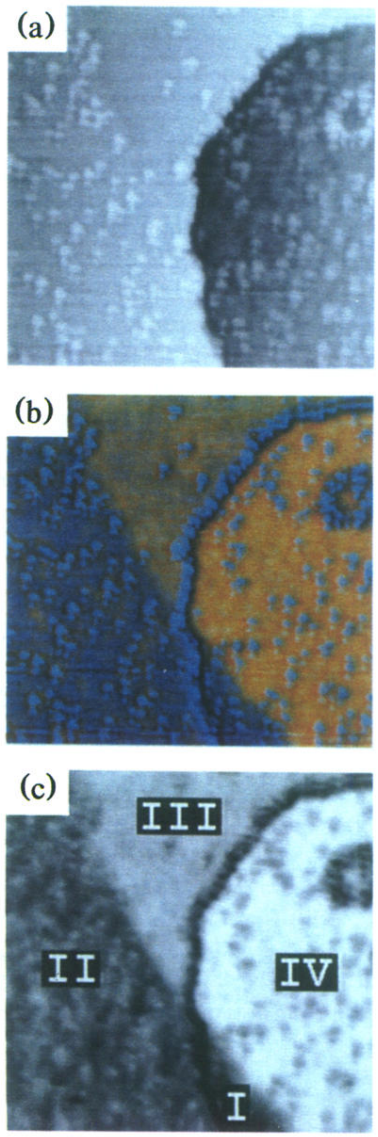

FIG. 3. STM and conductance images (360×360 Å) of type-*B* domains. (a) Topographic image, (b) overlay image (topography, blue; conductance, orange), and (c) conductance image at −0.6 eV, 1 nA. Type-*B* domains of varying thickness have been labeled I–IV.